Modelling Strategies for Simulating Delamination and Matrix Cracking in Composite Laminates

Frederic Lachaud, Christine Espinosa, Laurent Michel, Pierre Rahme, Robert Piquet

Modelling Strategies for Simulating Delamination and Matrix Cracking in Composite Laminates

Frederic Lachaud · Christine Espinosa · Laurent Michel · Pierre Rahme · Robert Piquet

Abstract The composite materials are nowadays widely used in aeronautical domain. These materials are subjected to different types of loading that can damage a part of the structure. This diminishes the resistance of the structure to failure. In this paper, matrix cracking and delamination propagation in composite laminates are simulated as a part of damage. Two different computational strategies are developed: (i) a cohesive model (CM) based on the classical continuum mechanics and (ii) a continuous damage material model (CDM) coupling failure modes and damage. Another mixed methodology (MM) is proposed using the contin uous damage model for delamination initiation and the cohesive model for 3D crack propa gation and mesh openings. A good agreement was obtained when compared simple charac terization tests and corresponding simulations.

Keywords Composite materials · Delamination · Finite element analysis · Crack propagation · Matrix cracking · Mixed mode

1 Introduction

The composite materials are becoming very important in the aeronautical construction. The new generations of aircrafts structures are predominantly using composite materials. Devel oping a predictive numerical composite damage model for a local and global behaviour of the structure is nowadays a growing interest for the industries. Accepted methodologies, using links between local stress distributions and global behaviour of aircrafts components, are not applied for composite structures and even more for large structures. The computational mechanics and the virtual testing are thought about as a solution to establish widely and cost

F. Lachaud (✉) · C. Espinosa · L. Michel · R. Piquet
ISAE ICA (Institut Clément Ader), Université de Toulouse, ISAE/DMSM, 10, Avenue Edouard Belin, BP54032, 31055 Toulouse Cedex 4, France
e-mail: frederic.lachaud@isae.fr

P. Rahme
Mechanical Engineering Department, Faculty of Engineering, Notre Dame University, P.O. Box : 72, Zouk Mikael, Zouk Mosbeh, Lebanon

effectively robust rules of design [1 3]. Currently, models involve damage mechanics for complex structures [4, 5].

Failure of composite structures due to external loading is a complicated process. This process includes intra and inter laminar damage and leads to stiffness loss [6]. The typical damage modes that lead to failure of composite laminates are matrix cracking, delamination and fibre breakage. To predict these mechanisms in composite structures, several authors develop a number of failure criteria. These criteria are based on either stress or strain analysis. In general, damage initiation occurs when first matrix cracking appears in composite materials and damage propagation such as delamination and fibre breakage leads to more serious damage. Puck et al. [7] proposed a composite material failure criterion to predict damage initiation and propagation for different damage modes. Pollayi et al. [8] modelled the first damage mode in composite helicopter rotor or wind turbine blades. They detect the matrix cracking using two failure criterion: matrix failure in compression and matrix failure in tension. Rebiere et al. [9] presented an energetic criterion to model initiation and propagation of matrix cracking and delamination in composite cross ply laminates. Moreover, Pavia et al. [10] used an energy analysis to predict the matrix cracking stress as a function of relevant material parameters. Van der Meer et al. [11] presented a finite element model using the phantom node method for matrix cracking and interface elements for delamination. Another model to predict the propagation of transverse cracks in polymer matrix composite laminates is proposed by Maimi et al. [12].

On the other hand, cohesive elements have increasingly used to simulate both delamination and matrix cracking. Shi et al. [13] developed a numerical model using interface cohesive elements to simulate matrix cracking. They assumed equally spaced cracks based on exper imental measurements and observations. Alvarez et al. [14] used two dimensional linear and quadratic cohesive elements to model crack initiation and propagation. Another delamination model using shell elements and a cohesive zone model is proposed by Borg et al. [15] in order to simulate DCB, ENF and MMB experiments. However, impact damage in composite materials is considered to be the most common and important damage form in aircraft structures. Impact on composite structures has been widely studied in the world [16, 17]. Several excellent books and texts have been already published devoted to fundamentals mechanics [18], to impact on composite structures [16, 17], to numerical related methods and models [19 21], to airworthiness and aircraft certification [22], or even to Virtual Testing [23]. Damage tolerance investigations for aeronautical applications have essentially been related to long term behaviour of airplane structures, then to fatigue life and fatigue crack propagation. Moreover, they have been connected to the strain energy released by damages (defined as cracks) under cyclic loading [24]. Damage can be considered in itself as cracks initiated and propagated by the impact, as material discontinuities [25]. Damage tolerance is related to failures modes. To predict the strength evolution during damage accumulation, it is necessary to determine the contribution of each failure mode and often to use micromechanical models to analyze the stress distribution [26].

In this paper, two different computational strategies are developed in order to simulate matrix cracking and delamination propagation. A first cohesive model (CM) based on the classical continuum mechanics is proposed. This model is developed in order to simulate the delamination propagation using a number of failure criteria. Iso parametric triangular or quadrangular cohesive elements are used in this model. Another continuous damage material model (CDM) is presented in this paper. This model is used for both matrix cracks initiation and delamination propagation by coupling failure modes and damage. Finally, a mixed methodology (MM) is proposed using the CDM for delamination initiation and the CM for 3D crack propagation and mesh openings.

2 Delamination Analysis

Delamination is considered as the major damage of a composite structure. Delamination splits the safe structure and makes it no more continuous thus dropping down the shear, bending and torque rigidities. For pre tests simulations and vulnerability analysis, delamination is not event taken into account. Numerical modelling of delamination is done for post test simulations when it is needed to reproduce finely the local stresses and explain what happened during the experimentations. The preferred modelling strategy for delamination over the world, for scientists as well as for engineers, is the cohesive method. This strategy is coherent in a mechanical (or physical) point of view both with the intrinsic nature of this damage as a crack/discontinuity/opening/loss of cohesion, and representative of its characteristic dimension. In a numerical point of view, it is also very simple either to use in the frame of the traditional continuum mechanics or with the Finite Elements Method. It is indeed easy to cut FE nodal links between adjacent elements used to model the adjacent plies. Then cohesive elements can easily be introduced in the knowledge and know how of numerical modelling.

Thousands of papers are available in the literature concerning cohesive methods or cohesive elements. The cohesive model (CM), that was developed here, is presented for two materials. Explanations given here concern the developed model only. However, what is presented has indeed a lot in common with other models. The key point here and the presented work are about how a numerical model avoiding fitting numerical parameters is derived and what could be done to obtain a desired mechanical behaviour.

2.1 Cohesive Model Approach (CM)

The equivalent crack concept was used to build cohesive models from damage models under certain assumptions concerning the form of the cohesive law. In order to do that, one would use the property that the area under the cohesive law is equal to the dissipated energy per unit area when the faces of the cracks are completely disconnected. The discontinuity can be introduced into the damaged material when some criteria are verified. It is generally admitted that the cohesive model represents, for composite laminates, the behaviour law of a thin layer. This layer would glued together adjacent plies through the thickness. The idea is to make this layer entirely responsible of the plies cohesion, and therefore of the structure cohesion. It is also accepted that some interfaces present a negligible risk of cohesion compared to others, for instance two adjacent 0° plies. This allows inserting cohesive layers only between a priori chosen interfaces to reduce the computation cost. The cohesive layer is often considered to have a linear behaviour up to a maximum admissible stress level. This stress corresponds to a maximum relative displacement of the adjacent plies, and is to be considered as a bonding threshold. When the layer has reached this maximum stress level, it is considered to be losing progressively its potential resistance. This is called “energy release”. Delamination is consid ered as crack propagation. The decreasing shape of the stress displacement curve describes the smoothness or the brittleness of the rupture between the adjacent plies. Depending of the crack propagation mode, the plies interface bond is loaded. Different energy release rates must be experimentally determined. They are used to derive the global stress displacement curve of the cohesive model.

The cohesive behaviour is developed in order to model damage under impact loading. It is inspired from Pinho’s model [27]. Damage is initiated through a quadratic criterion, and propagation follows a critical energy release rate criterion in mixed mode I, II and III. This model has been validated through comparisons of dynamic numerical modelling with exper imental tests measurements.

2.1.1 Cohesive Behaviour Development

In order to model delamination propagation, iso parametric triangular or quadrangular cohesive elements are used [28, 29]. These elements are pure displacement interface elements dedicated to the modelling of inter layers, separating standard structural elements. The interface element ensures displacements and stress transfers between adjacent faces (adjacent layers). It can be considered to represent a homogeneous resin layer to which isotropic or orthotropic material properties can be assigned. Various damage models can also be associated to the interface element in order to simulate more or less complex delamination damage mechanisms. For example, Fig. 1 shows a bilinear behaviour for tensile and compressive behaviours in order to model the crack opening mode (Mode I of Linear Fracture Mechanic). Figure 2 shows pure shear behaviour in order to model a pure shear mode (Mode II of Linear Fracture Mechan ic). When a compressive load arrives after a crack opening mode, the behaviour is pure linear. The dissipated energies in mode I or II are equal to the area under the curves. The percentage of energy is obtained by finding the ratio between total energy and local energy.

The specific free potential energy ϕ_d is assumed to be of the form:

$$\rho\phi_d(\delta, d) = \frac{1}{2}(1 \;\; d).\delta.K.\delta \tag{1}$$

Where: d and δ (state variables of the interface behavior law) are respectively the scalar damage variable and the difference between displacement of the connected nodes (connected layers). ρ is the mass density [30] and K is the stiffness of cohesive elements. Then, the associated variables in term of thermodynamic approach are respectively the stress σ and the elastic energy rate Y [18], as:

$$\rho\frac{\partial\phi_d}{\partial\delta} = \sigma = (1 \;\; d)K.\delta \tag{2}$$

$$\rho\frac{\partial\phi_d}{\partial d} = Y = \frac{1}{2}\delta.K.\delta \tag{3}$$

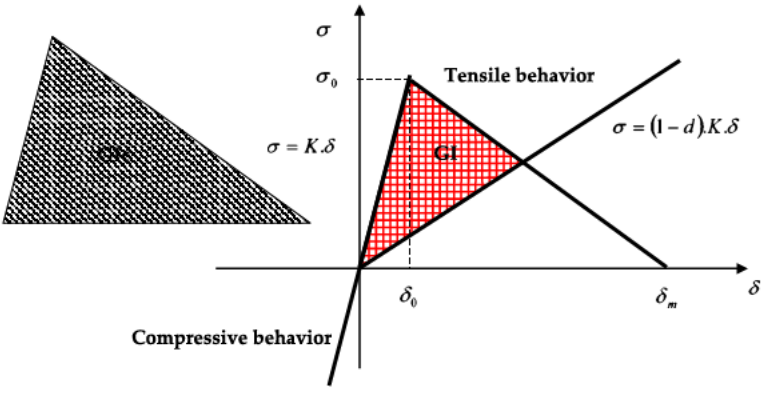

Fig. 1 Bi-linear cohesive behaviour: tensile-compressive behaviour

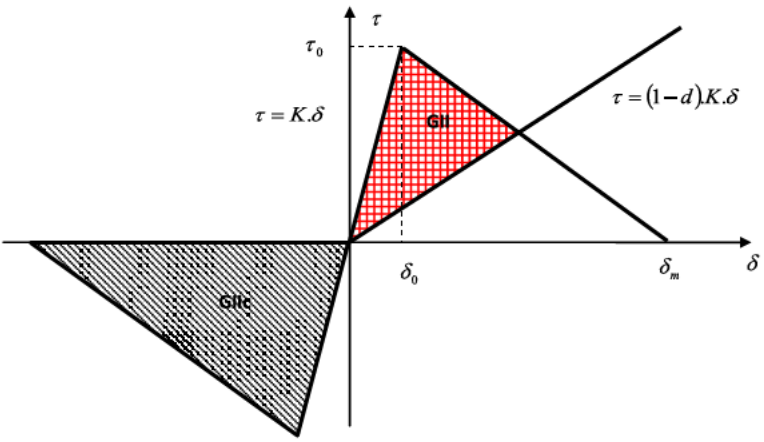

Fig. 2 Bi-linear cohesive behaviour: shear behaviour

Using the bilinear model (Figs. 1 and 2), damage development law can be computed as:

$$\begin{cases} \sigma = (1\ d)\ .\ K\ .\ \delta \\ d = \dfrac{\delta_m}{\delta_m\ \ \delta_0}\left(1\ \ \dfrac{\delta_0}{\delta}\right) \\ d = \ \min(d,1) \end{cases} \quad if\ \ \delta > \delta_0 \quad and\ \ d = 0\ \ else \tag{4}$$

With: $\delta_0 = \delta_{Ic} = \frac{\sigma_0}{K}$ and $\delta_m = \frac{2G_{Ic}}{\sigma_0}$

The displacement δ_0 of the cohesive finite element nodes, which initiates delamination, is given by a stress criterion. The failure displacement δ_m (when propagation occurs) is given by an energy criterion based on critical energy release rate in mode I, II and III (for 3D studies). The stiffness value K of cohesive elements is a parameter that influences the initial behaviour of delamination interface. For first studies, lot of authors [31, 32] give K=100,000 N/mm^3; it's a value that depends on numerical approach and could be fitted through correlation between the experimentation and the numerical models. Some other behaviour has been tested (Fig. 3). The damage law is given by either a sine or an exponential form. These behaviours can help to solve some convergence problem during implicit numerical approaches [33].

The damage behaviour for a sine law is given by:

$$\begin{cases} \sigma = (1\ d)\,.K\,.\delta \\ d = 1\ \left(\dfrac{\delta_0}{\delta}\right).\sin\left[\dfrac{\pi}{2}\left(\dfrac{\delta\ \ \delta_m}{\delta_0\ \ \delta_m}\right)\right] \\ d = \ \min(d,1) \end{cases} \quad if\ \ \delta > \delta_0 \quad and \quad d = 0\ \ else \tag{5}$$

The damage behaviour of cohesive element for an exponential law is given by:

$$\begin{cases} \sigma = (1\ d)\,.K\,.\delta \\ d = 1\ \exp\dfrac{\left(1\ \ \frac{\delta}{\delta_0}\right)^m}{m} \\ m = f\ (\delta_0, \delta_m) \\ d = \ \min(d,1) \end{cases} \quad if\ \ \delta > \delta_0 \quad and \quad d = 0\ \ else \tag{6}$$

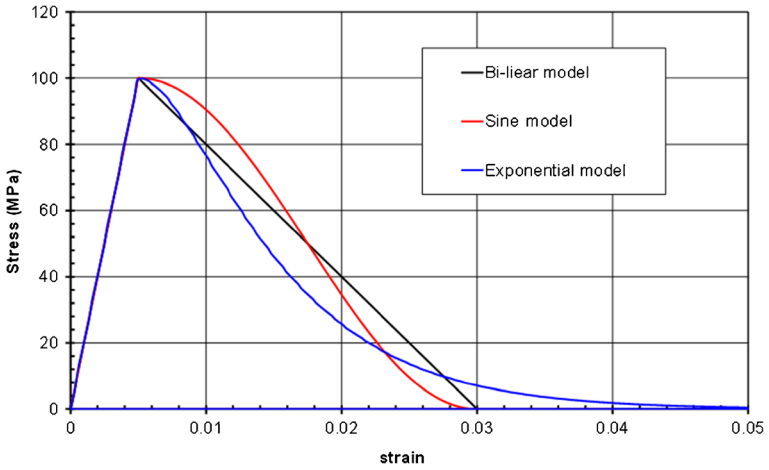

Fig. 3 Different shapes of cohesive behaviour law

The complete definition of the cohesive model is given by initiation and failure (propagation) displacements. Initiation is estimated with a quadratic stresses criterion given in Eq. (7). This criterion has been modified in order to couple normal and shear stresses (α scalar in Eq. 7). Moreover, this criterion takes into account the increase of shear strength when a compressive normal stress is applied. The initiation criterion (2D case) can be written as followed:

$$\sqrt{\left(\frac{\langle\sigma_{33}\rangle_+}{\sigma_{33}^R}\right)^2+\alpha^2\left(\frac{\sigma_{13}}{\sigma_{13}^R\left(1+\langle\sigma_{33}\rangle\ .\tan(\varphi)\right)}\right)^2}=1=\sqrt{\left(\frac{\sigma_{eq}}{\sigma_{eq}^R}\right)^2} \tag{7}$$

$$\text{With: } \begin{cases} \sigma_{33}=\ K_{33}.\ \delta_{33};\ \sigma_{13}=\ K_{13}.\ \delta_{13} \\ \sigma_{33}^R=\ K_{33}.\ \delta_{33}^0\ ;\ \sigma_{13}^R\ =\ K_{13}.\ \delta_{13}^0 \\ \sigma_{eq}=K_{eq}.\delta_{eq};\sigma_{eq}^R=K_{eq}.\delta_0;\delta_{eq}=\sqrt{\delta_{33}^2+\alpha^2.\delta_{13}^2};\alpha^2=\dfrac{K_{13}}{K_{33}} \end{cases}$$

$$\text{And } \begin{cases} \langle\sigma_{33}\rangle_+=\sigma_{33}\ \text{ if }\ \sigma_{33}\geq 0 \text{ else } \sigma_{33}=0 \\ \langle\sigma_{33}\rangle\ =\sigma_{33}\ \text{ if }\ \sigma_{33}<0 \text{ else } \sigma_{33}=0 \end{cases}$$

The coefficient φ is taken in order to increase the failure shear stress when normal compressive stress occurs and also to represent friction before the opening mode. A value of 10° is taken for φ in this study. Experimental tests are underway to further identify this parameter. The behaviour of cohesive element is assumed to be orthotropic. Two stiffness's are introduced K_{33}, K_{13}, in tensile and compressive behaviour, respectively. Finally, the displacement is obtained, when initiation of delamination in mixed mode I/II occurs, as:

$$\delta_0=\delta_{33}^0.\delta_{13}^0\left(1+\langle\delta_{33}\rangle\ .\tan(\varphi)\right)\sqrt{\frac{1+\alpha^2.\beta^2}{\left(\delta_{13}^0\left(1+\langle\delta_{33}\rangle\ .\tan(\varphi)\right)\right)^2+\left(\alpha\beta\delta_{33}^0\right)^2}} \tag{8}$$

With: $\beta=\frac{\delta_{13}}{\delta_{33}}$; $\alpha^2.\beta^2=\frac{G_{II}}{G_I}$

The propagation criterion, identified on the composites laminates [34, 35], is based on a mixed mode critical energy release rate expressed as a power law:

$$\left(\frac{G_I}{G_{IC}}\right)^{\eta}+\left(\frac{G_{II}}{G_{IIC}}\right)^{\eta}=1=\left(\frac{G}{G_C}\right)^{\eta} \tag{9}$$

With:
$$\begin{cases} G = G_I + G_{II};\ G_c = \dfrac{\sigma_{eq}.\delta_m}{2} \\ G_I = \dfrac{\delta_m^I \delta_0^I}{2\left(\delta_m^I - \delta_0^I\right)} K_{33}\left(\delta - \delta_0^I\right);\ G_{II} = \dfrac{\delta_m^{II} \delta_0^{II}}{2\left(\delta_m^{II} - \delta_0^{II}\right)} K_{13}\left(\delta - \delta_0^{II}\right) \\ \sigma_{eq} = \dfrac{K_{eq}.\delta_0.\delta_m}{2}; \end{cases}$$

The parameter η determines the shape of the criterion of delamination propagation in mixed mode. It is determined by testing the delamination propagation MMB in mixed mode [34, 35].

The global failure mixed mode resultant displacement is then:

$$\delta_m = \frac{2\left(1+\alpha^2\beta^2\right)}{\delta_0}\left[\left(\frac{K_{33}}{G_{Ic}}\right)^{\eta}+\left(\frac{K_{13}\alpha^2\beta^2}{G_{IIc}}\right)^{\eta}\right]^{\frac{1}{\eta}} \tag{10}$$

$\alpha^2\beta^2 = \frac{G_{II}}{G_I}$ is the coupling coefficient for an orthotropic cohesive law (K_{33} different from K_{13}).

Mathematical expressions of δ_0 and δ_m are different from Pinho's development [27] where the coupling coefficient is correct only for an isotropic interface. The increases of shear strength, when normal compressive stresses exist, are also not taken into account. This cohesive behaviour has been implemented in specific Matlab implicit/explicit finite element developments in order to obtain a robust behaviour. An example of deformed double cantilever beam (DCB) 2D model using four nodes finite elements with plane strain behaviour is showed in Fig. 4. This Matlab model is a generic model that can model double cantilever beam (DCB), end notched flexure (ENF), end loaded split (ELS) and mixed mode bending (MMB) tests specimens. This model is also developed for 3D application. The out plane shear stress σ_{23} is introduced into the initiation criterion and the critical energy release rate in mode III G_{IIIC} is integrated in the propagation criterion.

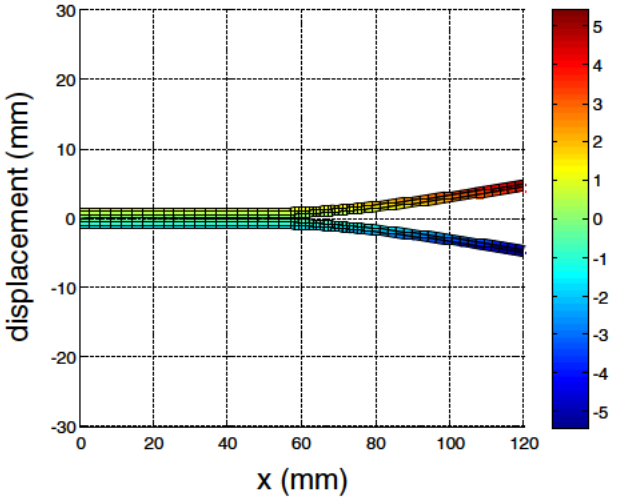

Fig. 4 Generic mesh of DCB specimen realized on Matlab

The choice of the model parameters, in particular of the interface stiffness's and failure of the opening and shear behaviour, has to be defined by getting consistent physical characteristics and meeting also some specific conditions (mode ratio). To summarize, the model parameters are:

- Stresses at initiation,
- Stiffness,
- Critical energy release rate in mode I and II,
- Shape of propagation criterion (η value),
- Length of cohesive element.

In order to obtain models less sensitive to the mesh refinement, a time delay effect (viscous behaviour) is introduced [36, 37]. Then, the damage is modified as:

$$\dot{d} = \frac{1}{\tau}\left(1 - \exp^{-a\langle ds - d\rangle_+}\right) \tag{11}$$

Where a and τ are the damage delay parameters, ds the damage computed in Eq. (4), and d the new damage variable. All these parameters are explained and discussed in the following paragraphs for mode I (DCB tests), mode II (ENF tests) and mode I+II (MMB tests).

2.1.2 Mode I: DCB Sample Behaviour

A specific code was developed for managing finite elements type (cohesive, quadrangular laminate finite elements), constitutive laws (bilinear, sine with or without plasticity), mesh refinement, implicit/explicit algorithm and boundary conditions. An example of 2D Finite elements model of DCB sample realized using the MatLab software is shown in Fig. 4. The load displacement behaviour of DCB specimen is presented on Fig. 5 for several initiation stresses with different values of τ_c (parameters for delay effect parameter). The parameter (a) is fixed at 1. The theoretical orthotropic beam analytical solution of load displacement DCB behaviour has been added to the figure as a reference.

A small value of initiation stress (5 MPa) fails to get the analytical peak load where the propagation starts. It allows the convergence of the model by passing the maximum load and creating the delamination propagation. A high stress initiation value (35 MPa) without delay effect fails to simulate the propagation of delamination; the Newton's algorithm diverges. The time delay effect allows solving the convergence problems. However, if the parameter value is high, it over estimates the stress initiation and doesn't respect the energy of propagation. It has been chosen to use a real (physical) value for stress initiation, equal to the transverse failure stress (σ_{22}), such that (σ_{22}) is equal to (σ_{33}) for unidirectional composite laminates.

Figure 6 shows, for the same numerical case, the influence of the stiffness and the length of interface. Concerning the stiffness K_{33}, a low value underestimates the initial stiffness of DCB sample but its influence remains low. On the contrary, the length of cohesive elements largely influences the initiation of delamination propagation for quasi static analysis (Fig. 6a). The mesh convergence is obtained for a length smaller than approximately 0.15 mm for this finite element model.

For rapid dynamic analysis (Fig. 6b), an important length of cohesive element generates oscillations of the load displacement curve when the propagation occurs [27]. This is due to

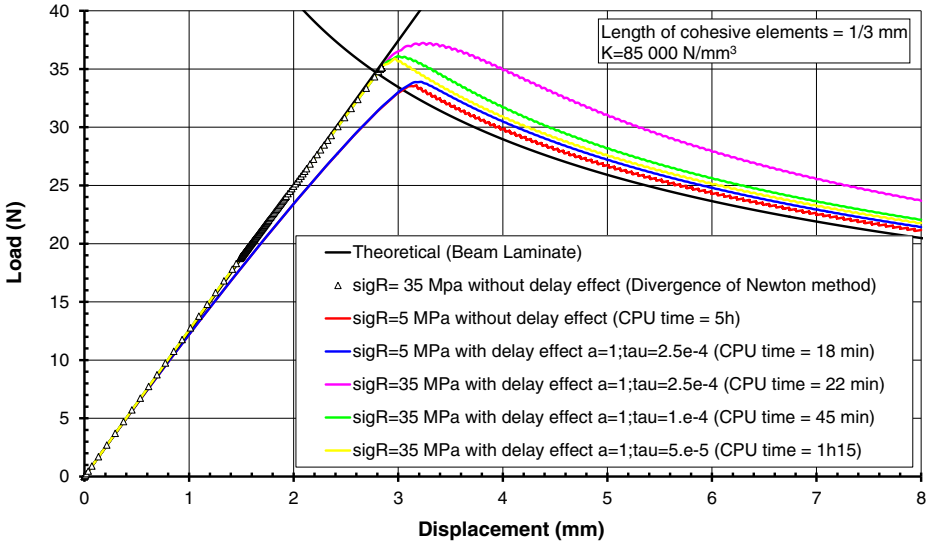

Fig. 5 Load-displacement behaviour of DCB test ; influence of initiation stresses and delay effect parameters, a_0 40 mm, G_{Ic} 0.12 N/mm, T300/914 laminate, 100 % 0° plies

the load jump when a cohesive element is completely damaged. These vibrations are also minimized by time delay effect application [35]. The length of cohesive elements conditions the number of damaged elements at the same time during the propagation part of the law behaviour curve (Fig. 3). An important length will cause to stiffen the global load displacement behaviour. For a sufficiently small length of cohesive elements, the length of crack represented by a number of damaged elements remains constant. Figure 7 shows an example of stresses (in MPa) and damage development for the first twenty cohesive elements (the first one is situated at the crack tip) versus time and for an explicit computation. During the initiation phase, the normal cohesive stress in safe elements has negative values and increases. The phase of initiation is also characterized by an increase of the damaged elements number, being stabilized in propagation phase, where it reaches a value of 14 elements for this computation. This corresponds to a crack length of 2.8 mm, a constant length during all the propagation phase (0.2 mm cohesive element length).

2.1.3 Mode II: ENF Tests

Mode II tests realized on ENF specimen have an unstable behaviour if the initial crack length is smaller than the half of the distance separating the supports. This is characterized by a sharp decline of the load during delamination propagation (Fig. 8). This phenomenon named “snap through” is characterized by a specific global behaviour. During propagation, for the same displacement, there are two load solutions. Figure 8 gives an example of behaviour in mode II for ENF test. The finite element model is the same as the DCB model; only boundary conditions changed. The behaviour model of the cohesive element is compared with the model developed by Allix et al. [38] and with the analytical solution [34], for 2D and 3D finite element computation. The global behaviour of the delamination propagation in mode II

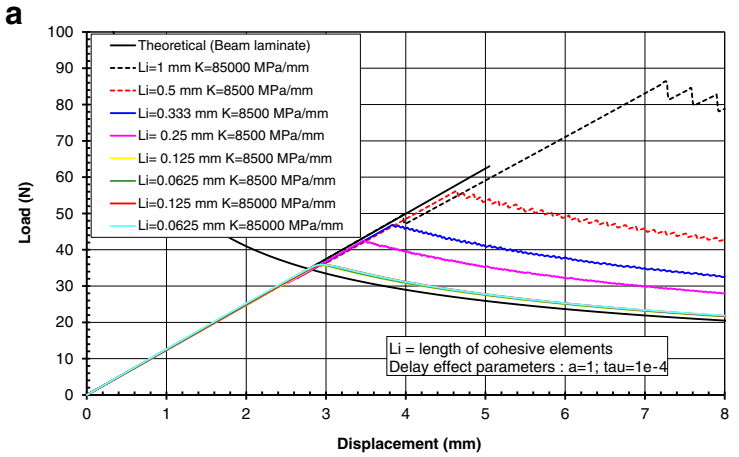

Numerical Quasi-Static behaviour: stiffness and length of cohesive element influence

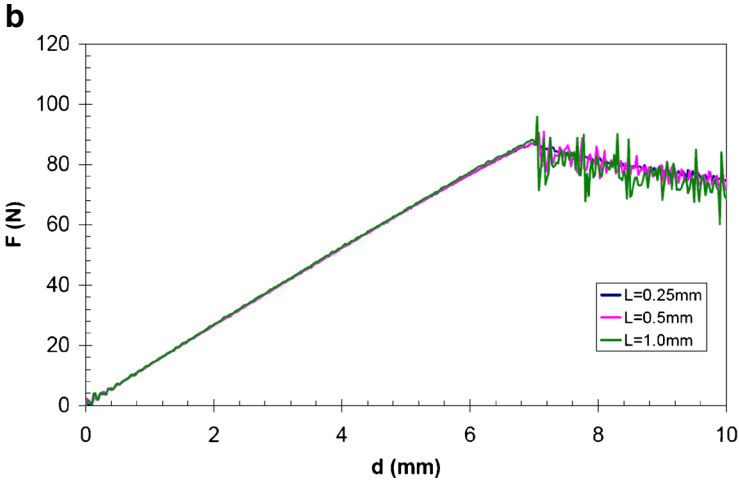

Explicit computation: length of cohesive element influence

Fig. 6 Load-displacement curves for DCB tests; stiffness and cohesive element length influences, a_0 40 mm, **a** G_{Ic} 0.12 N/mm, T300/914 material, 100 % at 0°, **b** G_{Ic} 0.765 N/mm, T800/M21 material, 100 % at 0°

is well transcribed by both models for 2D and 3D analysis. Allix's model slightly underesti mates the value of peak load. Only "Riks" algorithm is able to reproduce the theoretical solution ("snap through" effect).

2.1.4 Mixed Mode I+ II: MMB Tests

The developed cohesive behaviour law is aimed to be dependent of the mode. In order to respect the ratio between mode I and mode II, the data input must respect a certain condition. This condition imposes that the variation of the relationship, between the dissipated energy and the total energy, must be positive [32].

For the developed model, this condition can be written as follow:

$$\frac{\partial}{\partial\left(\alpha^2\beta^2\right)}\left(\frac{G_{dissipated}}{G_{critical}}\right)=\frac{\partial}{\partial\left(\frac{G_{II}}{G_I}\right)}\left(\frac{G_d}{G_c}\right)=\frac{\partial}{\partial d}\left(\frac{G_d}{G_c}\right)+\frac{\partial}{\partial\left(\frac{G_{II}}{G_I}\right)}\left(\frac{G_d}{G_c}\right)\geq 0 \qquad (12)$$

Where: $\frac{G_d}{G_c}=\frac{d}{\frac{\delta_m}{\delta_0}(1\ \ d)+d}$

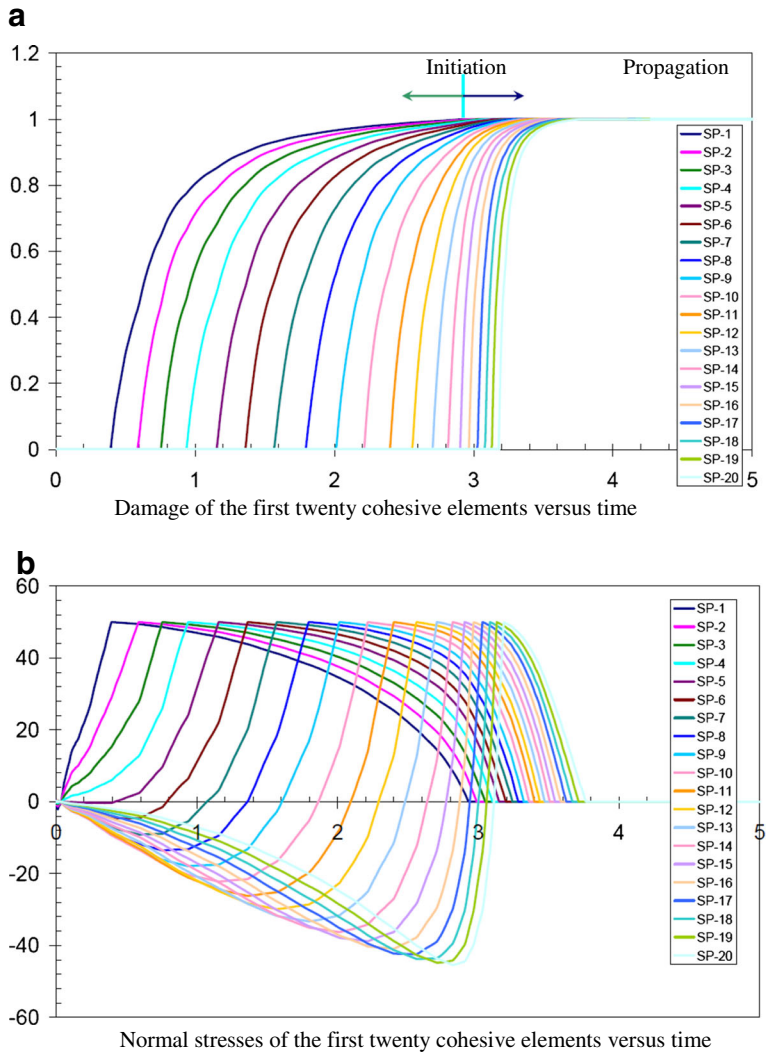

Fig. 7 Damage and normal stresses development versus time for an explicit computation DCB tests, T800/M21e material σ_r 50 MPa, G_{Ic} 0.765 N/mm, computation with DYNA FE Code

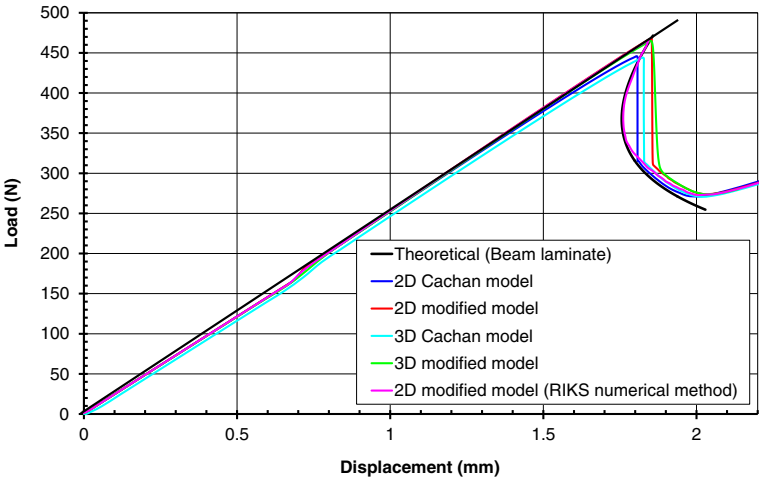

Fig. 8 Load-displacement behaviour of ENF tests (Mode II) for a T300/914 $[0]_{24}$ laminate: comparison between some cohesive models and theoretical approach

For example, for $\eta = 1$:

$$K_{13} = \left(\frac{G_{IC}}{G_{IIC}}\right).\left(\frac{\sigma_{13}^2}{\sigma_{33}^2}\right).K_{33} \tag{13}$$

Note that Eq. (13) is valid for some forms of initiation and propagation criteria. It remains valid for Benzzeggah Kenane criterion [39], and for the formulation described in this document. In the case of complex criteria, it is necessary to reformulate the criterion equation. The set data of the cohesive law is summarized in Table 1. Figure 9 shows the cohesive behaviour law for mixed mode observing the condition of modes interaction.

Allix's model [23] being formulated initially by taking into account Eq. (13), it is dependent of the mode opening. This model is also based on a criterion form which naturally respects the mode ratio. Figure 10 shows a comparison of the load displacement behaviour for a MMB test with 50 % of G_I, between Cachan model [23] and the modified proposed model. The solution obtained by the analytical beam approach is also given. The model data is indicated in Table 1. The respect of the condition between stiffness's and stresses serves to obtain a solution very close to the theoretical one. The model gives the same load displacement curve as Allix's model.

These developments will be implemented, in a subsequent work, in commercial software packages (SAMCEF, LS DYNA, ABAQUS software's) for quasi static and fast dynamics computation. Other formulations of the cohesive behaviour law were also developed, in particular a formulation with plasticity and strain rate effects.

Table 1 Data for cohesive element behaviour

K_{33}	K_{13} calculated	G_{IC}	G_{IIC}	σ_{33}^0	σ_{13}^0	η	φ
85,000 N/mm^3	75,000	0.35 N/mm	1.2 N/mm	50 MPa	80 MPa	1.2	10°

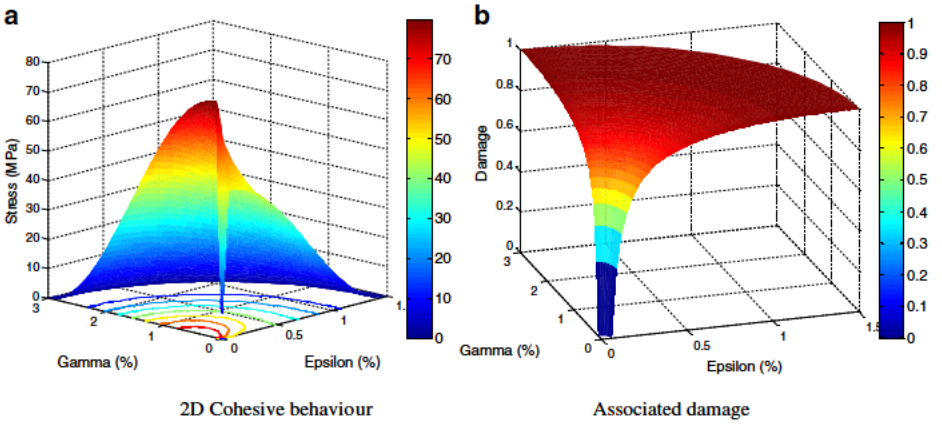

Fig. 9 Cohesive FE behaviour and damage development

2.2 Data Identification and Discussion

The cohesive behaviour parameters and the corresponding identification required tests are summarized in Table 2.

The critical energy release rate values and the criterion shape (η value) are given by the fracture mechanic tests in mode I, II and I+II respectively by DCB, ENF (or ELS) and MMB tests. The initiation stresses (σ_{33}, σ_{13} and σ_{23}) are determined by realizing specific tests:

- σ_{13} by inter laminar shear tests (Figs. 11b and 12),
- σ_{33} by 4 point bending L angle sample tests (Fig. 11a),
- σ_{23} is assumed to be equal to σ_{13}.

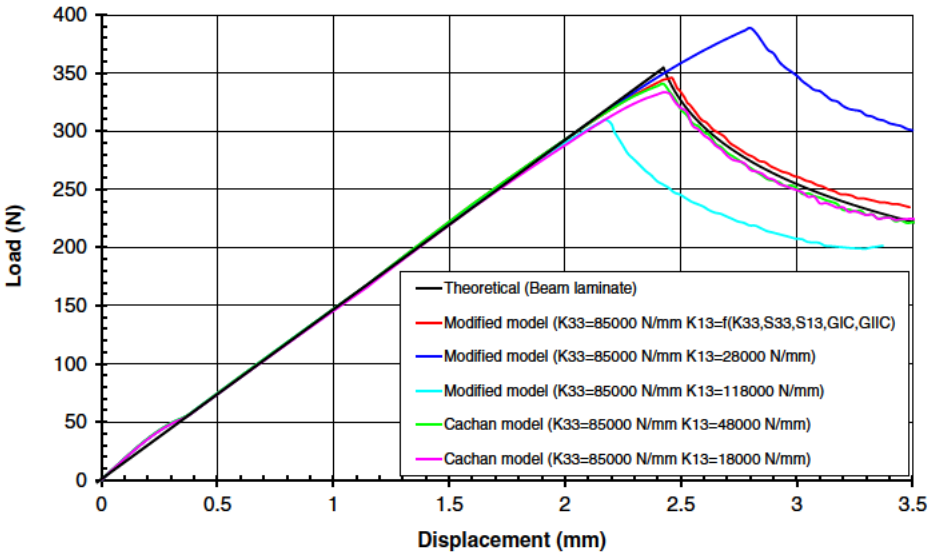

Fig. 10 Load-displacement curves for MMB test and for different models: cohesive element stiffness influence, T700GC/M21e UD laminate, G_{Ic} 0.545 N/mm, G_{IIC} 1.2 N/mm

Table 2 Summary of the cohesive input data behaviour and the associated tests

Critical energy release rate			Shape of propagation criterion	Stiffness of cohesive element			Initiation stresses			Delay effects	
G_{Ic}	G_{IIc}	G_{IIIc}	η	K_{33}	K_{13}	K_{23}	σ_{33}	σ_{13}	σ_{23}	a	τ
Fracture mechanics tests (DCB, ENF, MMB…)				Numerical and Fracture mechanics tests			L-angle 4 points bending test	Inter-laminar Shear tests (Fig. 11b)		Numerical and experimental tests	

The Stiffness's of the cohesive element are usually equal to 100,000 N/mm^3 [40]. However, a value in connection with the out of plane stiffness of the studied laminates is taken. A value of 85,000 N/mm^3 for an orthotropic behaviour of cohesive elements is used. K_{33} being fixed, K_{13} and K_{23} are calculated in order to respect the modes ratio using Eq. (13). Figure 13 shows the mode I strain energy release rate (G_I) as a function of the crack length a, and the crack length as a function of the opening displacement. The crack length was measured using two methods, (i) a microscope and (ii) KRAK GAGES from RUMUL. The critical strain energy release rate calculations are based on values obtained visually for quasi static tests. The initiation values of 450 J/m^2 and the propagation values of 800 J/m^2, for G_{IC}, have been reported by Prombut et al. [34] for the T700GC/M21e. These values are in close comparison with the conducted tests. A value of 765 J/m^2 for G_{IC} was chosen which gives the allowable values of 50 65 mm for a.

Table 3 gives the cohesive parameters values for T700GC/M21e and T800S/M21e com posite laminates.

The model validation is carried out initially on implicit and explicit finite element MATLAB numerical models for strain plan (2D) hypothesis. The model will be validated using commercial software packages (SAMCEF, LS DYNA, ABAQUS) for 3D compos ite laminates computations in a subsequent work. In order to obtain a numerical model valid for explicit computations of impact conforming to the hypotheses of mechanics and experimental conditions, a double cantilever beam (DCB) test case is investigated [27]. The finite element model and the influence of several numerical parameters (e.g. damping, hourglass control, applied displacement and applied velocity) have been investigated.

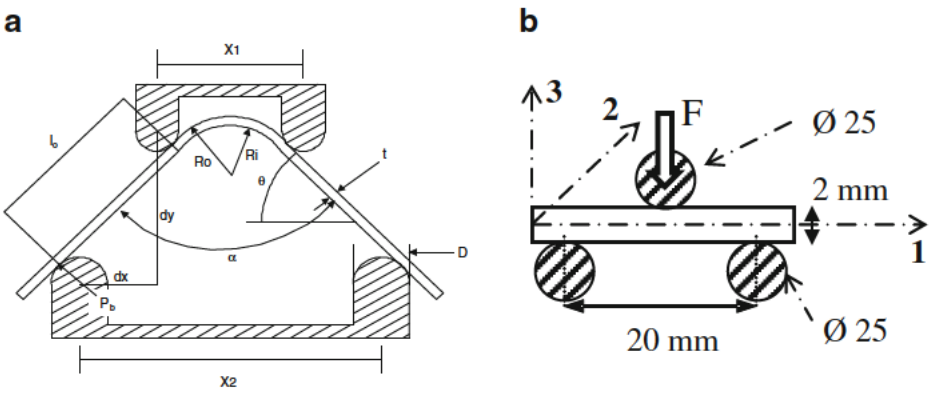

Fig. 11 a 4-point bending L-angle test; b Inter-Laminar Short Specimen 3-point bending test

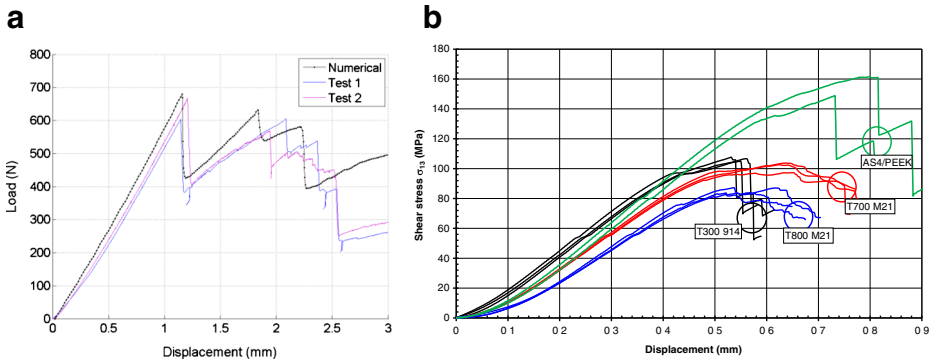

Fig. 12 **a** L-Shape 4 point bending behaviour of T700GC/M21 UD $[0°]_{24}$ laminates, **b** Inter Laminar Short Specimen behaviour of several UD laminates

3 Continuous Damage Model (CDM)

In this section, a ply damage model based on a failure criteria damage model is presented. The basic material model is the nonlinear elastic anisotropic homogenized continuum damage mechanics one developed by Matzenmiller et al. [41]. The original model emphasizes that the global anisotropy of the laminate does not change after damage, and that the ply remains elastic after damage. Thus, damage is modelled through its effect on the elastic rigidity loss in further loading or unloading until the damage reaches a value of 1 corresponding to failure.

3.1 Ply Damage Model

The model distinguishes 6 damage variables $\{d_i\}$, i=1,…,6 affecting the stiffness of the ply, and 5 failure modes $\{f_j\}$, j=1,…,5. The stress strain relationship can be written as:

$$\begin{Bmatrix} \varepsilon_{11} \\ \varepsilon_{22} \\ \varepsilon_{33} \\ \gamma_{12} \\ \gamma_{23} \\ \gamma_{13} \end{Bmatrix} = \begin{bmatrix} \frac{1}{E_{11}^0(1-d_1)} & \frac{\nu_{21}^0}{E_{22}^0} & \frac{\nu_{31}^0}{E_{33}^0} & 0 & 0 & 0 \\ \frac{\nu_{21}^0}{E_{22}^0} & \frac{1}{E_{22}^0(1-d_2)} & \frac{\nu_{32}^0}{E_{33}^0} & 0 & 0 & 0 \\ \frac{\nu_{12}^0}{E_{11}^0} & \frac{\nu_{23}^0}{E_{22}^0} & \frac{1}{E_{33}^0(1-d_3)} & 0 & 0 & 0 \\ 0 & 0 & 0 & \frac{1}{G_{12}^0(1-d_4)} & 0 & 0 \\ 0 & 0 & 0 & 0 & \frac{1}{G_{23}^0(1-d_5)} & 0 \\ 0 & 0 & 0 & 0 & 0 & \frac{1}{G_{13}^0(1-d_6)} \end{bmatrix} \begin{Bmatrix} \sigma_{11} \\ \sigma_{22} \\ \sigma_{33} \\ \sigma_{12} \\ \sigma_{23} \\ \sigma_{13} \end{Bmatrix} \tag{14}$$

Each failure criterion, given by Eqs. (15) to (19), is related to a specific failure mode and compares the state of stresses to the maximum allowable limit stresses.

- Tension/shear criterion

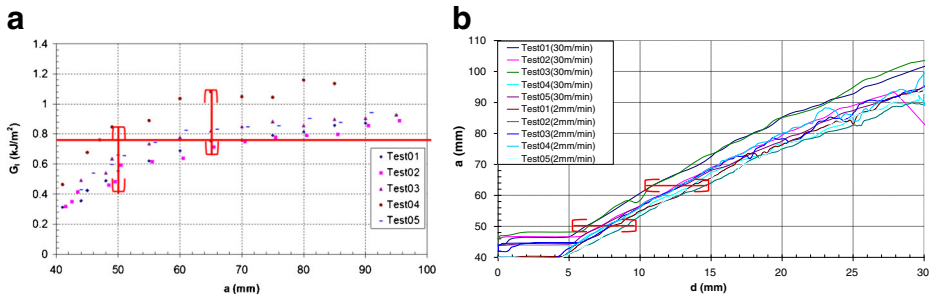

Fig. 13 **a** Strain energy release rate G_I vs. crack length a (LHS), **b** Crack length a vs. opening displacement d (RHS)

$$f_1(\sigma, r_1) = \left[\frac{\langle \sigma_{11} \rangle}{X_T}\right]^2 + \left[\frac{\sigma_{12}^2 + \sigma_{13}^2}{S_{fs}^2}\right] \; r_1^2 = 0 \tag{15}$$

- Compression criterion

$$f_2(\sigma, r_2) = \left[\frac{\langle \; 2\sigma_{11} + \langle \; \sigma_{22} \;\; \sigma_{33} \rangle \rangle}{2X_C}\right]^2 \; r_2^2 = 0 \tag{16}$$

- Crush criterion

$$f_3(\sigma, r_3) = \left[\frac{\langle \; \sigma_{11} \;\; \sigma_{22} \;\; \sigma_{33} \rangle}{3Z_C}\right]^2 \; r_3^2 = 0 \tag{17}$$

- Transverse cracking matrix criterion

$$f_4(\sigma, r_4) \quad \left[\frac{\langle \sigma_{22} \rangle}{X_C}\right]^2 + \left[\frac{\langle \; \sigma_{22} \rangle}{Y_C}\right]^2 + \left[\frac{\sigma_{12}}{S_{12} + \langle \; \sigma_{22} \rangle \tan\varphi}\right]^2 + \left[\frac{\sigma_{23}}{S_{23} + \langle \; \sigma_{22} \rangle \tan\varphi}\right]^2 \; r_4^2 \quad 0 \tag{18}$$

Table 3 Data for T300/914, T700GC/M21e and T800S/M21e (UD laminate) cohesive model behaviour

UD laminate	K_{33} (N/mm^3)	K_{13} (N/mm^3)	σ_{33} (MPa)	σ_{13} (MPa)	G_{Ic} (J/m^2)	G_{IIc} (J/m^2)	η
T300/914	100,000	f(K_{33})	35	60	125	400	1.0
T700GC/M21e	100,000	f(K_{33})	50	90	545	1,387	1.2
T800S/M21e	100,000	f(K_{33})	60	60	765	1,250	1.0

- Delamination criterion

$$f_5(\sigma, r_5) = \left[\frac{\langle \sigma_{33} \rangle}{Z_T}\right]^2 + \left[\frac{\sigma_{13}}{S_{13} + \langle\ \sigma_{33}\rangle \tan\varphi}\right]^2 + \left[\frac{\sigma_{23}}{S_{23} + \langle\ \sigma_{33}\rangle \tan\varphi}\right]^2\ r_5^2 = 0 \quad (19)$$

Where:

X_T and X_C	are respectively the tensile/compressive failure stresses in fibres direction
Y_T and Y_C	are respectively the tensile/compressive damage threshold stresses in direction 2
Z_T and Z_C	are respectively the tensile/compressive damage threshold stresses in direction 3
S_{12}, S_{23} and S_{13}	are the shear damage threshold stresses
$r_i \in [1, \infty]$	is called the limit load ratio.

And $\begin{cases} \langle \sigma_{ii} \rangle_+ = \sigma_{ii} \ \text{ if } \ \sigma_{ii} \geq 0 \text{ else } \sigma_{ii} = 0 \\ \langle \sigma_{ii} \rangle \ = \sigma_{ii} \ \text{ if } \ \sigma_{ii} < 0 \text{ else } \sigma_{ii} = 0 \end{cases}$

The effects of the strain rate (on failure/threshold stresses development) are achieved by the function:

$$\sigma_{ij} = \sigma_{ij}^{Stat}\left(1\ \ C_i \ln\frac{\dot{\varepsilon}}{\dot{\varepsilon}_{ref}}\right) \quad (20)$$

Where $C_i$and $\dot{\varepsilon}_{ref}$ are the material parameters. C_i and $\dot{\varepsilon}_{ref}$ are determined experimentally [33 35] using Hopkinson bar tests on $[\pm\alpha]_{3S}$ laminates (with α=0, 15, 30, 45, 60 , 75, 90).

At the undamaged state, the limit load ratio r_j of each failure criterion is set to 1. The limit load ratios are increased to take into account the current state of damage using the first thermodynamics principle. Indeed, each scalar function criterion f_j is considered to describe the admissible stresses envelop of the corresponding failure mode. All failure modes are supposed to be independent of each other. When the current computed stress state goes beyond the admissible stress envelop of a failure mode, the corresponding r_j is increased so that to scale back the stress to an admissible value (radial return onto the scalar function). An evolution function uses this updated value of r_j to compute the contribution of the correspond ing failure mode to the different damage variables. Since the behaviour is supposed elastic, scaling down the stress on the admissible envelop and scaling up the damage induced by the evolution of r_j must be coherent. It is easy then, using this condition, to derive several solutions for the evolution function (very similar to a generic form). In this study, the following expression, which is coherent with the assumptions of preserved elasticity and anisotropy after damage, is chosen to be used:

$$\phi_j(\sigma, d, \dot{\varepsilon}) = 1\ \ e^{\frac{1}{m}\left(1\ r_j^m\right)},\ r_j \geq 1 \quad (21)$$

This same form is chosen for all the failure modes evolution functions. Different parameters m is necessary. In these functions, parameters m can take into account the strain rate effects if desired (strain softening). The evolution of each damage variable d_i is considered to be due to some combinations of the ϕ_j contribution, as:

$$\dot{d}_i(\sigma, d, \dot{\varepsilon}) = \sum_{j\ \ 1}^{5} q_{ij}.\phi_j(m, r_j) \quad (22)$$

Thus, the parameters m can be seen as weighting factors of the related failure mode f_j on the induced damage d_i. The q_{ij} form a coupling matrix [q] between the failure modes evolution functions vector and the damage variables vector. Typical values of q_{ij} are 1 if the f_j failure mode evolution contributes to the increase of the damage variable d_i, 0 if not. The combination and the resulting coupling matrix have been derived from an experimental material characterization study. Tests were con ducted under quasi static loadings. The matrix [q] is given as:

$$[q] = \begin{bmatrix} 1 & 1 & 1 & 0 & 0 \\ 0 & 0 & 1 & 1 & 0 \\ 0 & 0 & 1 & 0 & 1 \\ 1 & 1 & 1 & 1 & 1 \\ 0 & 0 & 1 & 1 & 1 \\ 1 & 1 & 1 & 0 & 1 \end{bmatrix} \tag{23}$$

This model is used for both the initiation and the propagation of damage. The continuity and the coupling are the advantages of this damage modelling. It is obviously not possible to take into account the stress local concentrations, no discon tinuity is generated. However, the damage saturation and the coupling avoid changing the yield values of the stresses since they are updated at each damage state. Further more, mesh sensitivity is only related to the size of the element, not to the edges or face directions or shapes. A big counterpart of this model is that the damage variables are permanent but the behaviour remains elastic, same in tension and compression, thus no residual deformation can hold.

3.2 Data Identification of the Damage Development

In this paragraph, a summary of experimental tests realized in order to determine the model parameters of ply damage behaviour is presented. The identification procedure requires three experimental series of tests:

- Static tests to determine the failure stresses,
- Cyclic static tests to find the parameters characterizing the damage evolution, plasticity law, and damage thresholds,

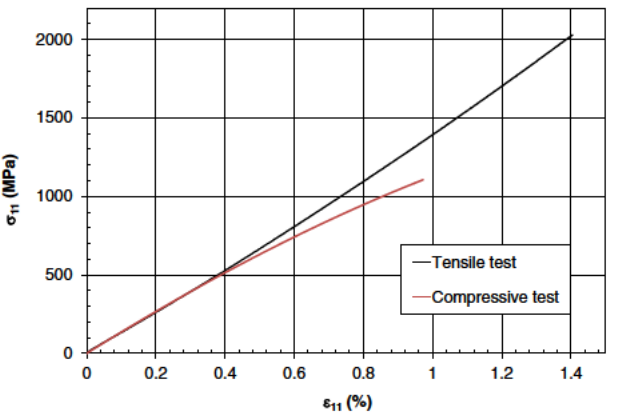

Fig. 14 Example of tensile/ compressive behaviour of T700GC/M21e [0°] laminates

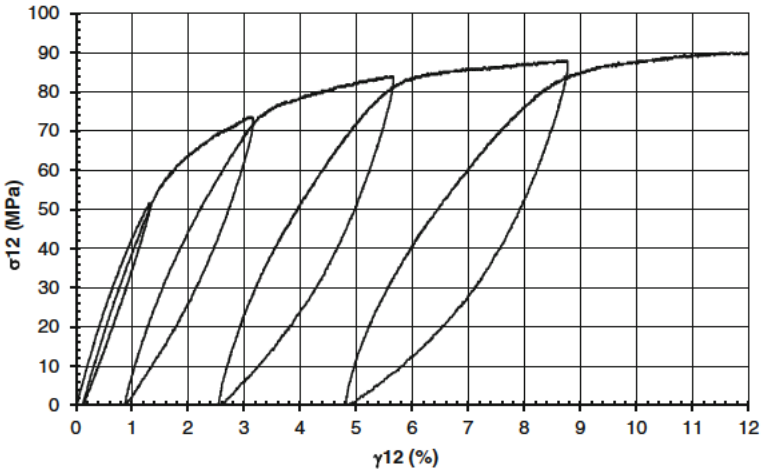

Fig. 15 Example of cyclic tensile behaviour of T700GC/M21e [0°] laminate

- Dynamic tests (Hopkinson tests) in order to characterize the strain rate effects.

3.2.1 Quasi static Behaviour

Static tests (T for tension and C for compression) were performed on $[0°]_8$ (T), $[0°]_{20}$ (C), $[90°]_{16}$ (T), $[90°]_{32}$ (C), $[45°]_{16}$ (T), $[45°]_{32}$ (T), $[\pm45°]_{2S}$ (T), and $[\pm45°]_{4S}$ (C) laminates. The specimen of unidirectional T700GC/M21e and T800S/M21e of dimensions 150×20 mm^2 (150 mm length and 20 mm width) are manufactured for tensile tests. Dimensions of 20×

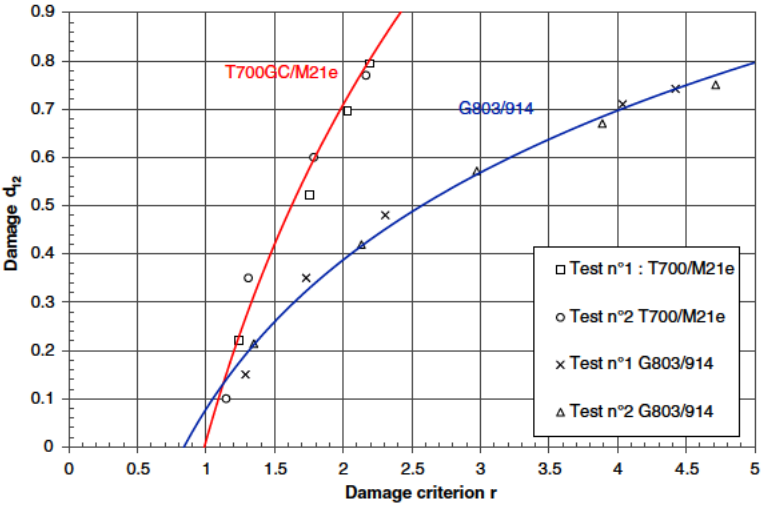

Fig. 16 Damage (d_4) versus criterion (r_4) curves for two composites laminates (an Unidirectional T700GC/M21e $[\pm45°]_{2S}$ laminate and a S5 woven $[\pm45°]_{2S}$ laminate G803/914)

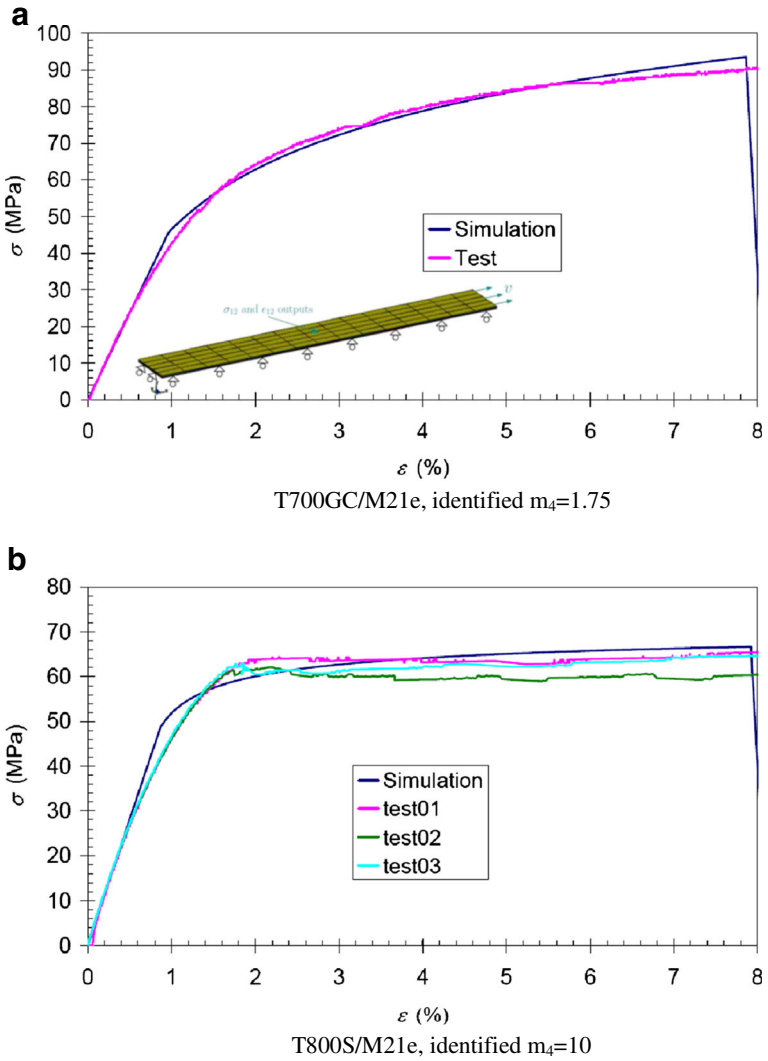

Fig. 17 Tests-Numerical comparison example behaviour of $[\pm 45°]_{2S}$ laminate for two type of composite laminates (explicit computation without strain rate effect)

10 mm^2 are taken for the compressive tests. The thickness of the specimen depends on the ply numbers. The ply thickness is about 0.25 mm. Two strain gages are stitched on each sample.

These tests are realized in order to determine the failure stresses and stiffnesses. Figure 14 shows an example of tensile/compressive behaviour of the T700GC/M21e. The stresses corresponding to failure are then obtained. Note that fibres tensile/compressive behaviour is not linear. For instance, the model didn't take into account this non linear behaviour and a linear behaviour is assumed. Cyclic static tests are performed to determine the parameters characterizing the damage evolution (m parameter). Two types of laminates are used: $[45°]_{16}$ and $[\pm 45°]_{2S}$. Compressive tests ($[45°]_{32}$) are realized in order to find an estimation of the

friction effect. Figure 15 shows an example of a quasi static cyclic tensile behaviour of a $[\pm 45°]_{2S}$ laminate.

For each cycle, the damage parameter d (d_4 in this case) and the criterion value (r_4 in this case) are determined. Figure 16 shows a specific curve of damage identification for T700GC/M21e and G803/914 $[\pm 45°]_{2S}$ laminates, obtained for cyclic static tests.

For a cyclic tensile test on a $[45°]_{16}$ laminate, we can separate the shear behaviour ($\sigma_{12}=f(\gamma_{12})$) can be separated from transverse behaviour ($\sigma_{22}=f(\varepsilon_{22})$). The coupled criterion (transverse cracking criteria of Eq. 18) is plotted versus damages variables d_2 and d_4. The parameters m_2 and m_4 can then be identified. Figure 17 illustrates the consistent identification obtained with this model for the in plane quasi static behaviour of two types of unidirectional composite materials.

3.2.2 Dynamic Damage and Failure

Dynamic compression tests have been conducted using a Split Hopkinson Pressure Bar test system at ISAE laboratory (Fig. 18), for strain rate effects identification, on various stacking sequences [33]. The experimental strain rates obtained vary from 200 (1/s) to 2000 (1/s).

The purpose of these tests is to characterize the behaviour of the T800S/M21e Unidirectional laminate for different fibres orientations compared to the axis of compression. Bars are made of stainless steel. The length of these bars is 2 m and the diameter is 20 mm. Square 20mmx20mm samples of $[\pm\theta]_{3S}$ were tested at angles of 15°, 30°, 45°, 60°, 75° at different strain rates in order to identify in one hand the effect of rates on the global behaviour, and on another hand, the contribution of the pure coupled loadings between inner ply fibres and matrix, and between plies interfaces. The dynamic behaviour of $[\pm 45°]_{3S}$ is a 4 parts stress strain curve (Fig. 19): the first part is linear (up to 1.2 % strain), the second is a curved part passing through a maximum stress (at about 2 % strain), the third part is a linear decreasing part with a strain rate dependent slope (from 3 % strain) and the fourth part is the failure at a strain increasing with the strain rate increasing (always $\leq$ 10 %).

The other angles do not exhibit the third part of the curves (Figs. 20 and 21). The apparent rigidities are all about 20GPa (±2 GPa depending on the strain rate). As for quasi static testing, using destructive analysis and previous studies observations [33], it is suggested that the second part is the coupling of inner and inter ply irreversible behaviour (onset of damage) and the third part is related to interfaces and parallel matrix cracking only present at [±45°]

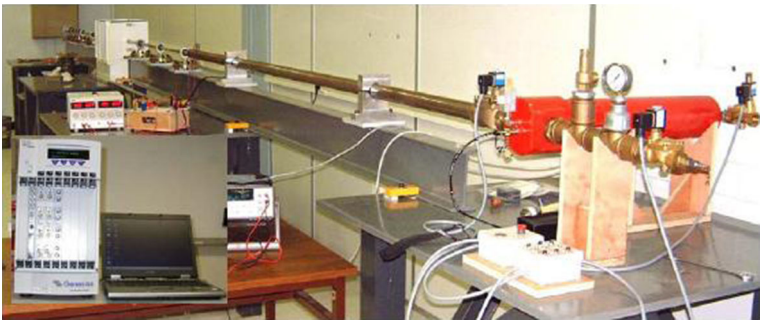

Fig. 18 Hopkinson's bars setup

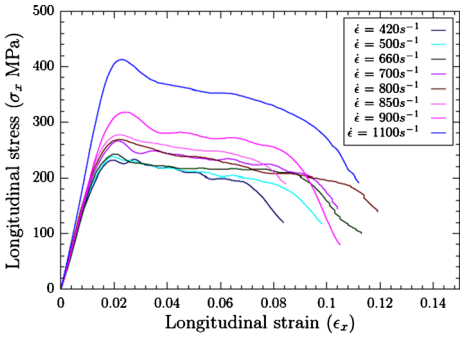

Fig. 19 Dynamic compression of T800S/M21e $[\pm 45°]_{3S}$

interfaces. It is suggested that the fourth part of the curves is related to damage saturation in the ply of T800S/M21e samples. Since the deformation yield is always the same, whatever the strain rate, it is supposed that the saturation damage is also the same. The growth of damage and the consequent maximum stress level in the second part of the curves are the strain rate dependent above a reference level.

For T800S/M21e composite laminate, the sensitivity of the strain rate is important for shear loading (Fig. 21a). On the contrary, the strain rate effect, for the fibres and the transverse direction, is fair less significant (Fig. 20). It is then possible to plot the strain rates effect curves. An example of the strain rate effect is given for the shear loading of T800S/M21e laminate on Fig. 22b.

3.2.3 Rate Effects in Compression: Input Data Identification

An example of experimental numerical comparison, achieved with LS DYNA software, is given in Fig. 23. Even though this model or some similar model already exist in commercial engineering software such as LS DYNA or ABAQUS, this model was implemented as a user defined material model in several commercial codes available for this study so that we are able to fit as desired the criteria, coupling matrix, and related material data.

Note that the model is also usable for woven composites but the failure/damage criteria are different. Table 4 resumes model data for T800S/M21e laminate. All out plane values (E_{33}, G_{13}, σ_{13} threshold, σ_{13} at failure…) are determined by applying the assumption of ply transverse isotropy (E_{33}=E_{22}, G_{13}=G_{12}…).

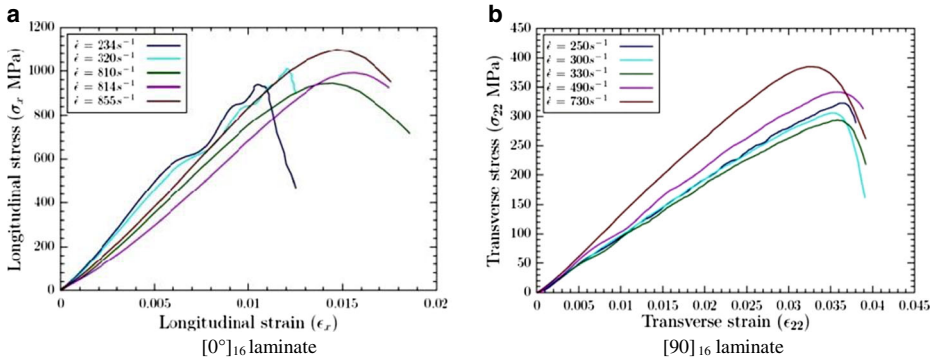

Fig. 20 Stress-Strain behaviour of $[0]_{16}$ and $[90]_{16}$ laminates versus strain rate, T800S/M21e

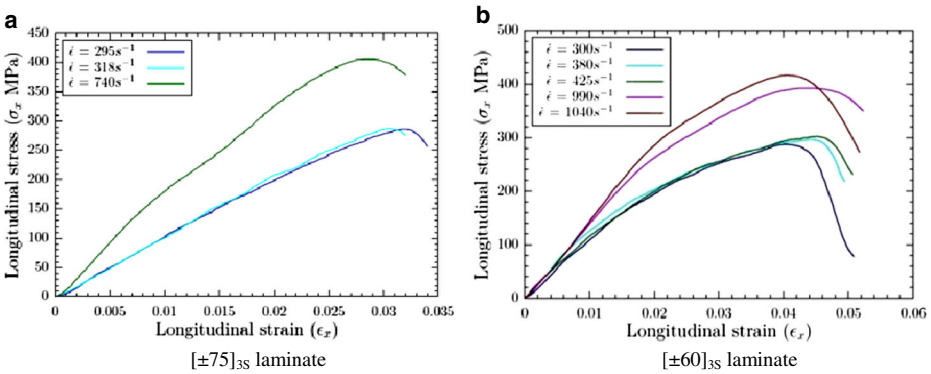

Fig. 21 Stress-Strain behaviour of $[\pm 75]_{16}$ and $[\pm 60]_{16}$ laminates versus strain rate, T800S/M21e

4 Discussion and Future Work

In this paper, a cohesive model (CM) based on the classical continuum mechanics is developed in order to simulate the delamination propagation using a number of failure criteria. This model is validated experimentally using DCB, ENF and MMB tests. Another model is developed to simulate both matrix cracks initiation and delamination propagation. This continuous damage material model (CDM) is coupling failure modes and damage. The input material data is identified by comparing simple characterization tests with the corresponding computer simulations. The details of experimental tests and numerical simulations are carried out to represent the CDM developed for Unidirectional plies behaviour.

In future works, a mixed methodology (MM) using the CDM for delamination initiation and the CM for 3D crack propagation will be tested. In this methodology, the ply transverse cracking development strongly influences the initiation and the propagation of delamination. The behaviour law of the plies is planned to initiate the damage cohesive interface elements as follows (Fig. 24):

- The matrix cracking criterion of the continuum damage model (criterion n°4, Eq. 18) for the brick elements is used as the damage initiation criterion of cohesive elements in the thickness of the plies;

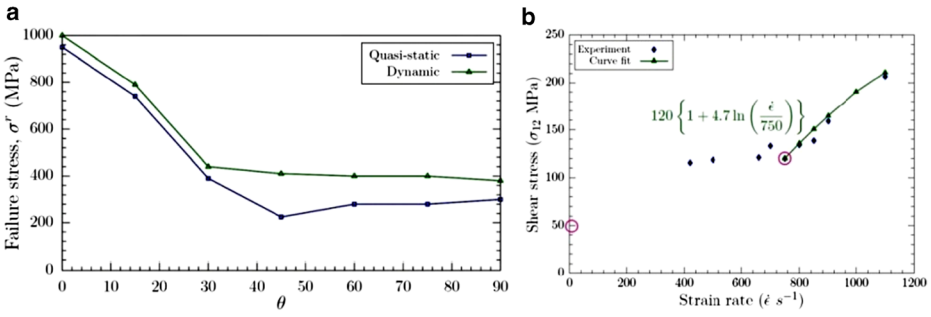

Fig. 22 **a** Static-dynamic comparison of failure stress versus laminate **b** Shear yield stress versus strain rate, T800S/M21e laminate

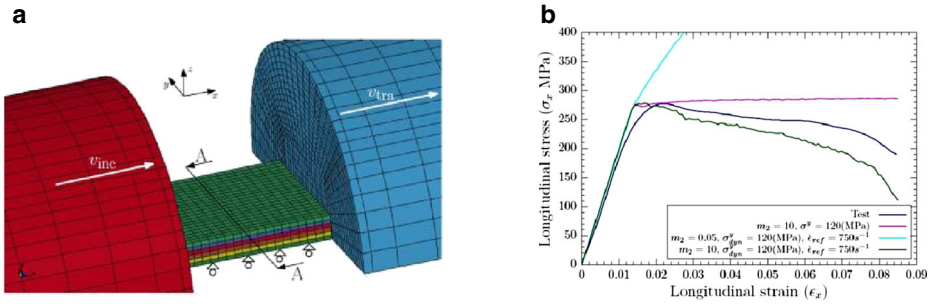

3D mesh of Hopkinson's test (explicit)

Stress-Strain behavior

Fig. 23 Experimental-numerical comparison of stress-strain behaviour for different strain rate, $[\pm 45]_{3S}$ T800S/M21e laminate

- The delamination criterion of the continuum damage model (criterion n°5, Eq. 19) for the brick elements is used as a delamination initiation criterion of the cohesive elements located between the layers.

For each criterion, the average of the values of the brick elements located on both sides of cohesive considered elements is used (Fig. 24). This allows obtaining a non local approach. The cohesive behaviour law concerning delamination is the one previously described. The cohesive behaviour law concerning transverse cracking is a bi linear model conveniently fitted for the values of failure energies: Accumulated energies are restored in order to determine the failure strains.

This coupled model is implemented in the explicit and implicit version (Europlexus, Mecano) of the finite element commercial software SAMCEF. Several authors modelled the macro cracks using specific spring elements [42, 43]. Bouvet's approach [43] inspired from Collombet et al. [44], uses spring elements to model matrix intra ply macro cracks and delaminations. These numerical approaches seem difficult to handle the spring's failure from impact experimentations. The proposed numerical finite element approach is close to the Lubineau approaches [42]. However, in this model, there is a virtual connection between the brick finite elements and the cohesive finite elements through the energy release rate criteria. This model is a mixture of the continuous (initiation) and the cohesive (propagation) models. The advantages and common disadvantages of both models are cumulated: damage coupling and matter opening, lack of explicit stress concentration due to surface openings. A huge computation CPU time can be circumventing using multiple cores machines. A generalization of this method is to model the material as a group of integration points connected together with cohesive local (DEM) or non local (SPH) forces and moments. Integration points can also be considered as representative elementary volumes. A mesh example of a composite laminate with cohesive elements is presented in Fig. 25.

Table 4 Data set for the proposed model and for T800S/M21e UD laminate

E_{11} 165 GPa	E_{22} 7.64 GPa	E_{33} 7.64 GPa	E_f 112 GPa	X_T 2.2 GPa	X_C 1.2 GPa
ν_{21} 0.0162	ν_{31} 0.0162	ν_{32} 0.4	m_i 10	Y_T 45 MPa	Y_C 280 MPa
G_{12} 5.61 GPa	G_{23} 2.75 GPa	G_{13} 5.61 GPa	Z_T 45 MPa	Z_C 0.7 GPa	S_{ffc} 0.5 GPa
S_{12} 0.05 GPa	S_{23} 0.05 GPa	S_{31} 0.05 GPa	S_{fs} 1.5 GPa	ω_{max} 0.87	φ 10°

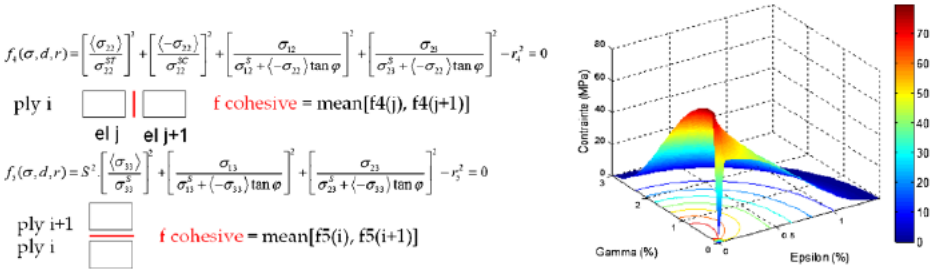

Fig. 24 Plies criteria to enable damage initiation of cohesive elements

In a subsequent work, the three developed models will be tested and applied on a numerical model for compression after impact of a local member as well as of global member. This will help to define a strategy to predict the residual strength when impacting for example an aircraft fuselage.

5 Conclusions

For the aeronautical companies, it is required to derive predictive numerical simulations for composite members, for assemblies, and in the same time, for the global structure. When simulating damage, the numerical simulations should be accurate to predict the location and the size of damages.

In this paper, two different damage models have been developed and a third methodology is proposed to be tested in a subsequent work. A first cohesive model (CM), that defines delamination as initially exiting, is based on the classical continuum mechanics. A second continuous damage material model (CDM) coupling failure modes and damage is also developed. Finally, a mixed methodology (MM) is proposed using the CDM for delamination initiation and the CM for 3D crack propagation and mesh openings. The input material data is identified by comparing simple characterization tests with the corresponding computer simulations.

The application of these models will be presented in a subsequent work. They will be tested on a local member as well as a global member such as an aircraft fuselage subjected to damage

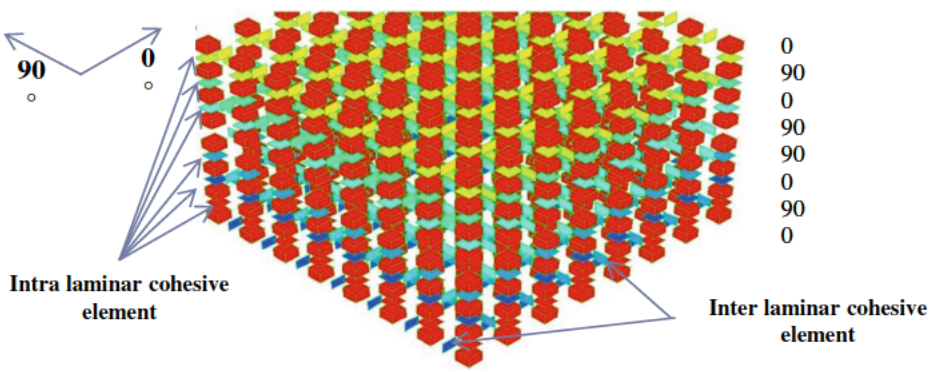

Fig. 25 Mesh example of $[(0/90)_2]_S$ laminate with cohesive elements in and between plies

impact. The comparison of the methods will be made in term of their capacity to predict the sample impact resistance. The advantages and disadvantages will be discussed when impacting a lab sample as well as an aircraft fuselage.

Acknowledgments The authors are grateful of Higher Education Commission of Pakistan for partial funding. Special thanks are also extended to IMPETUS Afea France as well as to all students and technical staff of ISAE for their valuable input towards numerical and experimental aspects, respectively.

References

1. Gaudin, J., Mahé, M., Grihon, S., Le-Roux, O.: Design optimization of composite Structures AIRBUS Challenges in MAAXIMUS. Workshop Giens 2009, 6 pp (2009)
2. Delsart, D., Joly, D., Mahé, M., Winkelmuller, G.: Evaluation of finite element modeling methodologies for the design of crashworthy composite commercial aircraft fuselage. 24th International Congress of the Aeronautical Sciences, Yokohama, Japan, (2004)
3. Fualdes, C., Morteau, E.: Composites @ Airbus Damage tolerance Methodology. FFA Workshop for the damage tolerance and maintenance. Composite Damage Tolerance & Maintenance Workshop, July 19 21, Chicago, IL, (2006). http://www.niar.wichita.edu/niarworkshops/Workshops/CompositeMaintenanceWorkshopJuly2006Chicago/tabid/99/Default.aspx. Accessed 10 Jan 2012
4. Windisch, M., Sun, D.-Z., Memhard, D., Siegele, D.: Defect tolerance assessment of Ariane 5 structures on the basis of damage mechanics material modelling. Eng. Fract. Mech. **76**, 59 73 (2009)
5. Bertolini, J., Castanié, B., Barrau, J.J., Navarro, J.P.: Multi-level analysis of skin/stringer debonding. ICCM17, Edimburgh, 27 31 July, United Kingdom, (2009)
6. Kashtalyan, M., Soutis, C.: Analysis of composite laminates with inter- and interlaminar damage. Prog. Aerosp. Sci. **41**, 152 173 (2005)
7. Puck, A., Schurmann, H.: Failure analysis of FRP laminates by means of physically based phenomenological models. Compos. Sci. Technol. **58**, 1045 1067 (1998)
8. Pollayi, H., Yu, W.: Modeling matrix cracking in composite rotor blades within VABS framework. Compos. Struct. **100**, 62 76 (2014)
9. Rebiere, J.L., Gamby, D.: A criterion for modeling initiation and propagation of matrix cracking and delamination in cross-ply laminates. Compos. Sci. Technol. **64**, 2239 2250 (2004)
10. Pavia, F., Letertre, A., Curtin, W.A.: Prediction of first matrix cracking in micro/nanohybrid brittle matrix composites. Compos. Sci. Technol. **70**, 916 921 (2010)
11. Van der Meer, F.P., Sluys, L.J.: Mesh-independent modeling of both distributed and discrete matrix cracking in interaction with delamination in composites. Eng. Fract. Mech. **77**, 719 735 (2010)
12. Maimi, P., Camanho, P.P., Mayugo, J.A., Turon, A.: Matrix cracking and delamination in laminated composites. Part II: Evolution of crack density and delamination. Mech. Mater. **43**, 194 211 (2011)
13. Shi, Y., Pinna, C., Soutis, C.: Interface cohesive elements to model matrix crack evolution in composite laminates. Appl. Compos. Mater. **21**, 57 70 (2014)
14. Alvarez, D., Blackman, B.R.K., Guild, F.J., Kinloch, A.J.: Mode I fracture in adhesively-bonded joints: A mesh-size independent modeling approach using cohesive elements. Eng. Fract. Mech. **115**, 73 95 (2014)
15. Borg, R., Nilsson, L., Simonsson, K.: Simulating DCB, ENF and MMB experiments using shell elements and a cohesive zone model. Compos. Sci. Technol. **64**, 269 278 (2004)
16. Abrate, S.: Impact on Composite Structures. Cambridge University Press, Cambridge (1998)
17. Richardson, M.O.W., Wisheart, M.J.Y.: Review of low-velocity impact properties of composite materials. Compos. Part A **27A**, 1123 1131 (1996)
18. Lemaitre, J., Chaboche, J.-L.: Mécanique des Matériaux Solides. Dunod, Paris (1988)
19. Liu, G.R., Liu, M.B.: Smoothed Particle Hydrodynamics A Meshfree Particle Method. World Scientific Publishing Co, Singapore (2003)
20. Shi, Y., Soutis, C.: A finite element analysis of impact damage in composite laminates. RAeS Aeronaut. J. **116**(1186), 1331 1346 (2012)
21. Shi, Y., Swait, T., Soutis, C.: Modelling damage evolution in composite laminates subjected to low velocity impact. Compos. Struct. **94**(9), 2902 2913 (2012)
22. De Florio, F.: Airworthiness an Introduction to Aircraft Certification. Butterworth-Heinemann Ed., 1st Edition, Oxford (2006)

23. Farahmand, B. (ed.): Virtual Testing and Predictive Modeling for Fatigue and Fracture Mechanics Allowables. Bahram Farahmand Editor, Springer, ISBN 978-0-387-95923-8 3, pp 459 (2009)
24. ASME: Damage Tolerance in Aricraft Structures. STP 486, ISBN O-8031-0072-8 (1971).
25. Reedy Jr., E.D., Mello, F.J., Guess, T.R.: Modeling the initiation and growth of delaminations in composite structures. J. Compos. Mater. **31**(8), 812 831 (1997)
26. Reifsnider, K.L., Case, S.W.: Damage Tolerance & Durability in Material Systems. Wiley-Intersciences, ISBN-10 0471152994 (2002)
27. Pinho, S.T., Iannucci, L., Robinson, P.: Formulation and implementation of decohesion elements in an explicit finite element code. Compos. Part A **37**, 778 789 (2006)
28. Alfano, G., Crisfield, M.: Finite element interface models for the delamination analysis of laminated composites: Mechanical and computational issues. Int. J. Numer. Methods Eng. **77**(2), 111 170 (2001)
29. Mi, Y., Crisfield, M., Davies, G., Hellweg, H.: Progressive delamination using interface elements. J. Compos. Mater. **32**, 1246 1272 (1998)
30. Cazes, F., Simatos, A., Coret, M., Combescure, A.: A cohesive zone model which is energetically equivalent to a gradient-enhanced coupled damage-plasticity model. Eur. J. Mech. A Solids **29**, 976 989 (2010)
31. Ilyas, M., Limido, J., Lachaud, F., Espinosa, C., Salaun, M.: Modélisation SPH 3D de l'impact basse vitesse sur plaque composite. 19ème Congrès Français de Mécanique, Marseille. France, (2009)
32. Turon, A., Camanho, P.P., Costa, J., Renart, J.: Accurate simulation of delamination growth under mixed-mode loading using cohesive elements: Definition of interlaminar strengths and elastic stiffness. Compos. Struct. **92**, 1857 1864 (2010)
33. Lachaud, F.: Contribution à L'analyse Multi Échelle du Comportement Non Linéaire Matériau des Structures Composites. Habilitation à Diriger des Recherches, Université de Toulouse, France (2011). http://oatao.univ-toulouse.fr/5165/
34. Prombut, P., Michel, L., Lachaud, F., Barrau, J.J.: Delamination of multidirectional composite laminates at 0°/θ° ply interfaces. Eng. Fract. Mech. **73**(16), 11 (2006)
35. Ilyas, M.: Damage modelling of carbon epoxy laminated composites submitted to impact laoding. PhD thesis, Université de Toulouse, ISAE, France, (2010)
36. Allix, O., Blanchard, L.: Mesomodeling of delamination: Towards industrial applications. Compos. Sci. Technol. **66**, 731 744 (2006)
37. Lachaud, F.: Prévision de L'endommagement de Composites Stratifiés Carbone-Epoxy Sous Chargement de Type Impact. 17ème Journée Nationales sur les Composites, Poitiers, 15 17 Juin. France, (2011)
38. Allix, O., Ladevèze, P., Corigliano, A.: Damage analysis of interlaminar fracture specimens. Compos. Struct. **31**, 61 74 (1995)
39. Benzeggagh, M.L., Kenane, M.: Measurement of mixed-mode delamination fracture toughness of unidirectional glass/epoxy composites with mixed-mode bending apparatus. Compos. Sci. Technol. **56**, 439 449 (1996)
40. Hamitouche, L., Trafaoui M., Vautrin A.: Modélisation du délaminage par la méthode de la zone cohésive et problèmes d'instabilité, 16ème Journées Nationales sur les Composites, (2009)
41. Matzenmiller, A., Lubliner, R.L., Taylor, A.: A constitutive model for anisotropic damage in fiber composites. Mech. Mater. **20**, 125 152 (1995)
42. Lubineau, G., Ladeveze, P.: Construction of a micromechanics-based intralaminar mesomodel, and illustrations in ABAQUS/Standard. Comput. Mater. Sci. **43**, 137 145 (2008)
43. Bouvet, C.: Etude de l'endommagement dans les structures composites. Mémoire d'Habilitation à Diriger les Recherches (2009)
44. Collombet, F., Lalbin, X., Lataillade, J.L.: Impact behavior of laminated composites: Physical basis for finite element analysis. Compos. Sci. Technol. **58**, 463 478 (1998)